Stereoselectivity of 8-OH-DPAT toward the serotonin 5-HT$_{1A}$ receptor: Biochemical and molecular modeling study

Joanna Dabrowska [a], Michal Brylinski [b,c,*]

[a] Department of Pharmacology, Medical University of Silesia, 38 Jordana Street, 41-808 Zabrze, Poland
[b] Department of Bioinformatics and Telemedicine, Collegium Medicum, Jagiellonian University, 17 Kopernika Street, 31-501 Krakow, Poland
[c] Faculty of Chemistry, Jagiellonian University, 3 Ingardena Street, 30-060 Krakow, Poland

ARTICLE INFO

ABSTRACT

The great majority of pharmacological investigations of 5-HT$_{1A}$ receptors' reactivity has been performed using racemic 8-OH-DPAT, therefore the biochemical as well as behavioral profiles of both 8-OH-DPAT enantiomers are not circumstantiated. In the biochemical study capability of racemic 8-OH-DPAT (0.05, 0.1 mg/kg s.c.) and its counterparts R-8-OH-DPAT (0.05, 0.1 mg/kg s.c.) and S-8-OH-DPAT (0.05, 0.1 mg/kg s.c.) to influence 5-HT synthesis rate in rats' prefrontal cortex, hypothalamus, hippocampus and brainstem was evaluated by HPLC/ED technique. Biochemical results are supported by the exhaustive computational study of possible differences between R- and S-enantiomer toward the 5-HT$_{1A}$ receptor. A reliable 3D model of the rat 5-HT$_{1A}$ receptor was constructed from the amino acid sequence using the crystal structure of bovine rhodopsin as a structural template. The structure of the receptor model was validated through docking studies and molecular dynamics simulations that gave results consistent with experimental data. Docking studies and the dynamics of ligand–receptor complexes emphasized different profiles of both enantiomers at the molecular level. The results of both biochemical and computational studies confirmed that R-enantiomer in contrast to S-8-OH-DPAT acts as full and potent agonist, whilst racemic form may display similar pharmacological profile to R-8-OH-DPAT.

© 2006 Elsevier Inc. All rights reserved.

MD, molecular dynamics
MM, molecular mechanics
energy minimization
MRN, median raphe nucleus
PFC, prefrontal cortex
TMH, transmembrane helix

1. Introduction

8-OH-DPAT is a prototypical 5-HT$_{1A}$ receptor agonist [1]. During the last 25 years 8-OH-DPAT was extensively used for pharmacological research to evoke variable biochemical effects of 5-HT$_{1A}$ receptors' activation: decrease of synthesis, turnover [2] and release of 5-HT in different animals' brain regions [3] as well as to cause different behavioral responses: hypothermia [4], hyperphagia [5], "5-HT$_{1A}$ syndrome" [6], mydriasis [7], spontaneous tail-flicks [8], etc. 8-OH-DPAT is a stereoselective compound. Generally, it is thought that R-8-OH-DPAT acts as a full and potent 5-HT$_{1A}$ receptor agonist, whereas S-8-OH-DPAT behaves as a partial agonist [9]. However, Hadrava et al. [10] reported that at postsynaptic 5-HT$_{1A}$ receptors in hippocampus both isomers act as partial agonists, because they antagonize suppressant effect of 5-HT.

Although R- and S-8-OH-DPAT have similar binding affinities to the 5-HT$_{1A}$ receptors in the rat hippocampus [11] as well as to the cloned human 5-HT$_{1A}$ receptors [12], their efficacies are different [9]. They behave differently in forskolin-stimulated adenyl cyclase assay in rat hippocampal membranes, since R-isomer could decrease the cAMP production to the same extent as 5-HT itself, whereas its S-counterpart acts as a partial agonist as it reduces cAMP levels to about 50% of the maximal reduction induced by 5-HT [9]. R-8-OH-DPAT had also higher efficacy in stimulation of human 5-HT$_{1A}$ receptor-mediated G protein activation *in vitro* (with a maximal effect of 90% relative to that of 5-HT) than S-isomer (57%), whereas racemic form (R,S-8-OH-DPAT) displayed intermediate efficacy [12]. Hadrava et al. [10] also reported, that R-enantiomer possess a two-fold greater potency than its S-counterpart to activate 5-HT$_{1A}$ receptors mediating suppression of hippocampus CA3 pyramidal neurons firing. These findings are also consistent with data suggesting that R-8-OH-DPAT has greater potency in inhibiting the biosynthesis of 5-HT compared to S-isomer [1,13,14]. Also differences in these compounds' behavioral profiles in the murine elevated plus-maze test [15], hypothermia [4,10] and monosynaptic reflex in rats [16] may indicate different intrinsic activity of both enantiomers at 5-HT$_{1A}$ receptors. It is also noteworthy that enantioselective HPLC assay in rats' biological fluids produced evidence that the chirality of both stereoisomers is fully maintained *in vivo* [17]. No enantiomeric interconversion was observed from R- to S-8-OH-DPAT or *vice versa*, but the significant difference in clearance indicates a stereoselective mechanism of elimination.

It is well known that 5-HT$_{1A}$ receptors located presynaptically on the soma and dendrites of the 5-HT neurons of the midbrain raphe nuclei, are involved in the effective inhibitory control of serotonergic neurons activity [18–20]. Stimulation of the somatodendritic 5-HT$_{1A}$ autoreceptors by a specific agonist, e.g. 8-OH-DPAT causes a neuronal hyperpolarization, decreases 5-HT cells firing rate, synthesis and turnover of 5-HT as well as release within raphe nuclei and subsequently within serotonergic projection areas [21]. The biochemical experiment has been focused on the assessment of any possible difference at the level at presynaptic 5-HT$_{1A}$ receptors between racemic 8-OH-DPAT and its active stereoisomer R-8-OH-DPAT as well as S-8-OH-DPAT known to be partial agonist. Therefore the capability of racemic 8-OH-DPAT and its R- and S-stereoisomers to modify 5-HT synthesis rate was determined by HPLC/ED technique by assay of 5-hydroxy-tryptophan (L-5-HTP) accumulation after aromatic amino acids decarboxylase inhibitor (NSD 1015) administration [22].

Molecular modeling techniques provide useful information on structural and functional aspects of G-protein-coupled receptors (GPCRs) and their interactions with ligands. GPCRs are membrane spanning receptors that mediate most of their intracellular actions through pathways involving activation of G-proteins. The high resolution crystal structure of bovine rhodopsin [23] provided for the first time a detailed atomic description of a GPCR molecule and represents a solid basis for modeling the structures of other rhodopsin-like GPCRs [24]. Such models have been extensively used to examine receptor interactions with ligands, providing hypotheses concerning structural determinants specifying high-affinity binding, selective binding or differences in binding of ligands [25]. The combined use of molecular modeling approaches, site-directed mutagenesis and biochemical studies gave detailed insight into molecular mechanisms of receptor folding, receptor activation, G-protein coupling, and regulation of GPCRs.

In the absence of 3D structures of 5-HT receptors, the model of rat 5-HT$_{1A}$ receptor was constructed by comparative modeling approach and used to simulate the molecular dynamics of ligand–receptor complexes. The optimization of transmembrane domain packing was carried out in the presence of explicit methane molecules, mimicking the non-polar environment of the membrane. The simulation technique, where the membrane environment is replaced by explicit methane molecules, is a fast and reliable method that appears to reproduce several important characteristics of membrane-embedded proteins [26–30]. A reliable 3D model of the rat 5-HT$_{1A}$ receptor was used to study the interactions with both enantiomers of 8-OH-DPAT, the estimation of their binding affinities and free energies of binding to the receptor. Moreover, the analysis of the possible differences in their binding modes was performed.

Although fundamental difference between these chiral compounds has already been indicated [13,31,32], the majority of pharmacological research has been performed using the racemic form of 8-OH-DPAT rather than its enantiomers.

The growing body of pharmacological reports emphasizes the importance of using stereoselective compounds instead of the racemic 8-OH-DPAT for biochemical and behavioral studies on 5-HT$_{1A}$ receptor function. To summarize, R-8-OH-DPAT displays greater efficacy than S-isomer in biochemical as well as in behavioral testing, which clearly suggests stereoselectivity in their intrinsic activities [9,14]. Therefore the purpose of the present investigation was to gain insight into how the enantiomers of 8-OH-DPAT exert their biological effects. Molecular modeling studies were undertaken in order to explain the phenomena of the stereo-structure-key to their intrinsic activities and biochemical study was addressed to investigate the possible difference between R- and S-isomer as well as the racemate at the presynaptic 5-HT$_{1A}$ receptors' level.

2. Materials and methods

2.1. Experimental procedures

2.1.1. Animals
Biochemical assay was conducted in rats, weighing 280–300 g. Before the experiment the rats were housed in groups of six in cages in a temperature-controlled room with free access to food and water and maintained under a 12 h/12 h light/dark cycle (light on 7.00). Each group of the experiment consisted of six animals, with the exception of control-saline group (12 rats). Local Bioethical Committee approved the experiment (permission #15/04, issued on 28 April 2004).

2.1.2. Drugs
NSD 1015 (m-hydroxybenzylhydrazine dihydrochloride), R-8-OH-DPAT hydrobromide (R-8-hydroxy-2-(di-n-propylamino)-tetralin), S-8-OH-DPAT hydrobromide and R,S-8-OH-DPAT hydrobromide were purchased from Sigma Chemicals, St. Louis, MO, USA. All substances were dissolved in 0.9% NaCl solution (saline). Saline, R-, S- and R,S-8-OH-DPAT were injected subcutaneously (s.c.), whilst NSD 1015 was administered intraperitonally (i.p.). 8-OH-DPAT pharmacophores were injected in the volume of 1 ml/kg, whilst NSD 1015 was administered in 2 ml/kg. Doses of above compounds are expressed as bases.

2.1.3. 5-HT synthesis rate
5-HT synthesis rate after aromatic amino acids decarboxylase inhibitor (NSD 1015) injection was determined in prefrontal cortex (PFC), hippocampus (CA), hypothalamus (HP) and brainstem (BS) of rats by HPLC/ED technique [33]. 5-HT synthesis rates were estimated after administration of saline, full and potent 5-HT$_{1A}$ agonist R-8-OH-DPAT (0.05, 0.1 mg/kg), partial 5-HT$_{1A}$ agonist S-8-OH-DPAT (0.05, 0.1 mg/kg) and racemic 8-OH-DPAT (0.05, 0.1 mg/kg). All substances were administered 15 min before NSD 1015 (100 mg/kg). Thirty minutes after NSD 1015 administration animals were sacrificed by decapitation and their PFC, CA, HP and BS were immediately dissected on an ice-chilled plate and weighed. The tissues were stored in deep freeze (−70 °C) pending assay. The tissue samples were homogenized in ice-cold 0.1 M perchloric acid (HClO$_4$) containing 0.05 mM ascorbic acid.

After centrifugation (15,000 × g, 20 min), the supernatants were filtered through 0.2 μm cellulose membranes (Titan-MSF Microspin Filters, Lida Manufacturing Corp.) and were injected into the HPLC system. Chromatography conditions—pump: model 302 HPLC with manometric model 802C (Gilson, France); precolumn: Hypersil BDS C18, 10 mm × 4 mm, 3 μm (Thermo-Quest, GB); column: Hypersil BDS C18, 250 mm × 4 mm, 6 mm, 3 μm (ThermoQuest, GB); injector: model 2175 rheodyne inert injector 20 μl loop (USA); flow rate: 0.7 ml/min; mobile phase: 75 mM NaH$_2$PO$_4$·2H$_2$O (Avocado Res. Chem.), 1.7 mM 1-octanosulfonic acid (Avocado Res. Chem.), 5 μM EDTA (Avocado Res. Chem.), 100 μl triethylamine/1 l (Sigma), 9.5% acetonitrile (Lab-Scan), pH 3.5 with phosphoric acid (Fluka). Detector conditions—detector: model 141 electrochemical detector (Gilson, France) with applied potential: +750 mV; output voltage: 1 V; gain: 10 nA, filter settings 5 s. Levels of 5-hydroxytryptophan (L-5-HTP) were expressed as pg/g of wet tissue. 5-HT synthesis rates (pmol/g/h) were calculated according to Carlsson et al. [22].

2.1.4. Data analysis
In chromatographic assay 5-HT synthesis rates (pmol/g/h) were presented as means ± S.E.M. and agonists treatment effects were examined by analysis of variance (ANOVA one-way) followed by Newman–Keul's for post hoc analysis; $p < 0.05$ was accepted as a statistically significant effect.

2.2. Molecular modeling

All calculations involving molecular mechanics (MM) energy minimization and molecular dynamics (MD) simulation were performed using Sander module of AMBER7 [34] and ff99 all-atom force field [35]. A Coulombic potential on the grid of 1 Å was calculated by LEaP (AMBER7) in order to place chloride ions at positions of the highest electrostatic potential around a protein molecule to neutralize it. To counteract the charge of the entire receptor model bearing a ligand molecule, a total of 14 chloride ions have been added, whereas 7 anions were required to exclusively neutralize the transmembrane domain. Bond constraints were imposed on all bonds involving hydrogen atoms with the SHAKE algorithm [36]. Long-range non-bonded interactions were truncated by using a 12 Å cutoff (electrostatic and vdW). The time-step length was 2 fs and the non-bonded pair list was updated every 10 steps. At every 1000 steps the translational and rotational motion was removed. The MD trajectories were analyzed with Carnal monitoring the RMS deviation of Cα and visually inspected with the VMD graphical software [37].

Docking procedures were carried out using AUTODOCK [38] in a 20 Å × 20 Å × 20 Å cube surrounding the putative binding site of the rat 5-HT$_{1A}$ receptor, allowing only conformational freedom to the ligand. Each exploration procedure consisted of 100 independent runs of genetic algorithm (GA) using the default options for the GA parameters.

2.2.1. Modeling of ligands
The initial structures of protonated R-8-OH-DPAT and 5-HT were constructed using InsightII [39]. An initial structure of S-8-OH-DPAT was constructed from the R-enantiomer by reversion of the chiral center. MOPAC7 program [40] with

AM1-BCC [41] set of parameters was used for geometry optimization and charge calculation with the aid of Antechamber [42]. In MD simulations the parameters were used in conjunction with the general Amber force field (GAFF) [43].

2.2.2. Localization of transmembrane part

The sequence of rat 5-HT$_{1A}$ receptor [44] was retrieved from the SwissProt sequence database [45]. The positions of seven transmembrane helices in the receptor sequence as well as in bovine rhodopsin were taken from the multiple sequence alignment of 506 GPCRs sequences (class: A—rhodopsin like, family: amine) provided by GPCRDB (information system for G-protein-coupled receptors) [46].

2.2.3. Construction of seven-helix bundle

The helical bundle of the bovine rhodopsin [23] was used as a structural template to build a model of the helical part of rat 5-HT$_{1A}$ receptor by homology. The sequence of each helix was aligned with that of the corresponding helix of rhodopsin. Amino acids of rhodopsin were mutated to those of the rat 5-HT$_{1A}$ receptor to construct an initial structure. The side chains were built by SCWRL3, a rotamer library search method to minimize the energy of steric clash [47].

2.2.4. Initial refinement of seven-helix bundle

The crude structures of transmembrane helices bundle (without connecting loops and terminals) of 5-HT$_{1A}$ receptor was refined by MM and MD simulation. Energy refinement was done by 1000 cycles of steepest-descent minimization followed by 1000 cycles of full-conjugate gradient minimization. MD simulations were performed for backbone atoms constrained at their energy-minimized positions with a 10 kcal/mol/Å^2 force constant. The system was heated to 500 K for first 10 ps then gradually cooled to 100 K for 500 ps with long temperature scaling. For the last 10 ps, the temperature was decreased to 0 K and the model was further refined by unconstrained energy minimization.

2.2.5. Identification of natural agonist binding site

The results from site-directed mutagenesis experiments [48,49] were used as guidelines in the docking of 5-HT into the central cavity of the 5-HT$_{1A}$ seven-helix bundle model. The exploration was limited to the region containing the residues experimentally known to be primarily involved in an agonist binding. The position of 5-HT with the lowest energy of binding reported by AUTODOCK was used in further simulations. Subsequently, the transmembrane domain of the 5-HT$_{1A}$ receptor containing 5-HT docked into the putative binding site was subjected to optimization in a strongly hydrophobic environment. The purpose of this action was to obtain the optimized structure of seven-helix bundle of 5-HT$_{1A}$ receptor in the active conformational state.

2.2.6. Optimization of the translational and rotational orientation of the helices

The optimization of mutual orientation of seven transmembrane helices and the optimization of helical bends and kinks were carried out in a strongly hydrophobic environment formed by methane molecules. The structure of seven-helix bundle of 5-HT$_{1A}$ receptor model bearing 5-HT molecule was

placed in a rectangular box containing 3591 methane molecules. The size of the box was 73.05 Å × 67.59 Å × 55.30 Å Å resulting in a volume of 273046.84 Å^3 and a density of approximately 0.5 g/cm^3. The density of the methane box is not the density observed in the hydrophobic core of the membrane bilayer [50] due to the different equilibrium distance between carbons in the methane box and in the polycarbon chain of the lipids [26]. Moreover, the higher density of the methane box may lead to short contacts between molecules and thus extreme behavior of the system [26]. Initially, the atoms of the receptor were kept fixed, while the methane molecules were energy minimized (1000 cycles of steepest-descent followed by 1000 cycles of conjugate gradients), heated to 300 K in 100 ps and equilibrated for 200 ps. Subsequently, the entire system was subjected to 500 ps of MD simulation in 300 K at constant volume using particle mesh Ewald method to evaluate electrostatic interactions [51]. A dielectric constant of $\varepsilon = 1$ has been used since an explicit solvent produces the required dielectricity on its own accord. To preserve the helical conformation of transmembrane helices during molecular dynamics simulations, distance restraints were applied between the backbone oxygen atom of residue n and the backbone nitrogen atom of residues $n + 4$, excluding prolines. It has been suggested that interhelical hydrogen bonds in methane are stronger than in water and the bond distances are shorter [26,52], therefore lower and upper bounds of hydrogen bond restraints were set to 2.5 and 3.2 Å, respectively. Every 1 ps the structures were collected for analysis.

The total hydrophobic area (ASA$_H$) of the receptor model was calculated as follows:

$$\text{ASA}_\text{H} = \sum_{i=1}^{N} \text{ASA}_i \times H_i$$

where ASA$_i$ is the accessible solvent area of ith residue, H_i the standardized value of hydrophobicity for ith residue according to Eisenberg scale of hydrophobicity for amino acids [53], and N is the total number of residues. The accessible solvent area of each residue was calculated using Surface module of Jackal program [54].

2.2.7. Construction of loops and terminals

The conformations of N- and C-terminal as well as second extracellular loop (ECL2) of 5-HT$_{1A}$ receptor were modeled with the aid of MODELLER8v1 [55] using the corresponding fragments of bovine rhodopsin [23] as structural templates. The sequence alignments were done using ClustalW1.83 [56] (Gap Opening Penalty: 10.00, Gap Extension Penalty: 0.20, Delay divergent sequences: 30%, Protein weight matrix: Gonnet series). The backbone structures of remaining loops were built by RAPPER [57], an ab initio conformational sampling method in dihedral space. For each loop the set of 1000 conformers was generated and the best conformation was chosen based on RAPPER scoring function. The side chains of terminals and loops were optimized using SCWRL3.

The third intracellular loop (ICL3) of the rat 5-HT$_{1A}$ receptor consists of 116 amino acids, therefore this loop needed a special treatment. The structure of ICL3 was predicted from the amino acid sequence using ROBETTA (full-chain protein structure prediction server) [58]. Additionally, the possibility of

disulfide connectivity existence was examined for the ICL3 sequence by a disulfide bridges predictor DISULFIND [59].

Loops and terminals were connected to the helical bundle and the entire 5-HT$_{1A}$ receptor model was subjected to an energy refinement procedure.

2.2.8. Energy refinement of entire receptor model

The raw structure of 5-HT$_{1A}$ receptor model bearing 5-HT molecule was energy-refined by MM and MD simulation. A strongly hydrophobic environment formed by methane molecules may unsuitably affect the conformation of loops and terminals, therefore the environment was partially compensated by setting a dielectric permeability ε equal to $4r$ (where r is the inter-atomic distance in Å) in the absence of an explicit solvent. During MD simulation loops and terminals were allowed to move, whereas the atoms of TMHs as well as 5-HT were constrained with a 10 kcal/mol/Å^2 force constant. Minimization was carried out for 2000 steps before MD simulation (1000 cycles of steepest-descent followed by 1000 cycles of conjugate gradients). For MD simulations the molecule was heated to 450 K for 40 ps then gradually cooled to 300 K for 100 ps. Subsequently, the entire system was subjected to 1 ns of MD in 300 K to optimize the packing of extra- and intercellular parts of 5-HT$_{1A}$ receptor model. The atomic coordinate sets collected for the last 100 ps of simulation were used to calculate an average structure, which finally was energy-minimized in 2000 steps.

Site-directed mutagenesis studies of GPCRs have shown that a pair of cysteines being highly conserved among all GPCRs, forms a disulfide bond [60,61]. The disulfide bond between C109 in TMH3 and C187 in ECL2 was present during all calculations.

2.2.9. Docking of R- and S-8-OH-DPAT

The similar exploration procedure as described for the docking of 5-HT was performed for R- and S-8-OH-DPAT separately and the position of each ligand with the lowest energy of binding was used in further simulations.

2.2.10. MD simulations of receptor–ligand complexes

To prevent unfolding and undesirable deformations of the TMHs as well as to produce rigid helix body motions as observed in experimental studies [62], distance restraints $O(n)$–$N(n + 4)$ were applied as described previously. Solvent effects were included by using a distance-dependent dielectric function ($\varepsilon = 4r$) for the reasons given previously. A similar strategy for constraining the transmembrane helices together with a dielectric permeability of $\varepsilon = 4r$ has been used previously during molecular dynamics simulations of G-protein-coupled receptor models [63,64]. The coordinates were saved at every 1 ps. MD simulations of receptor–ligand complexes consisted of the following steps:

1. Initial unconstrained energy minimization procedure (1000 cycles of steepest-descent minimization followed by 1000 cycles of full-conjugate gradient minimization).
2. One hundred picoseconds of MD during which the temperature of the system was gradually raised from 0 to 300 K. The receptor–ligand complex was constrained to its energy-minimized structure by a weak potential of 0.5 kcal/mol/Å^2.
3. Two hundred picoseconds of MD at constant temperature during which the ligand was constrained to its energy-minimized position by a potential of 0.05 kcal/mol/Å^2, allowing the protein to accommodate the ligand. To prevent the premature conformational changes of the receptor until the system became fully equilibrated, the two terminal Cα atoms of each TMH were constrained with a 0.05 kcal/mol/Å^2 force constant.
4. Production run including two different protocols:
    4.1. One nanosecond of unconstrained MD at 300 K.
    4.2. One nanosecond of MD at 300 K during which the ligand was constrained by a very weak potential of 0.005 kcal/mol/Å^2. The results obtained for this protocol are denoted 'ligand-constrained'.
5. The atomic coordinate sets collected for the last 100 ps of production run were used to calculate an average structure, which finally was energy-minimized in 2000 steps (1000 cycles of steepest-descent minimization followed by 1000 cycles of full-conjugate gradient minimization).

2.2.11. Estimation of affinity value and free energy of binding

The estimation of the affinity value (K_i) as well as the free energy of binding (E_{bind}) of R- and S-8-OH-DPAT toward the rat 5-HT$_{1A}$ receptor was done using AUTODOCK facility. The energy-minimized average structure of each receptor–ligand complex after MD simulations was used for the redocking of the ligand into the central cavity of the 5-HT$_{1A}$ receptor model. Cluster analysis was performed and structurally similar multi-member clusters were outputted. A cluster including the positions of ligand corresponding to the one present in the energy-minimized average structure of receptor–ligand complex was identified based on the reference RMSD values and further used in the calculation of standard deviation and the mean value of estimated affinity and free energy of binding.

3. Results and discussion

3.1. Molecular modeling

3.1.1. 5-HT$_{1A}$ receptor modeling

The process of the rat 5-HT$_{1A}$ receptor model construction started from identifying membrane spanning helices based on the multiple sequence alignment and further modeling of the transmembrane domain. The start and end positions of TMHs in the model were found to be: F33-I61 (TMH1), V70-L99 (TMH2), G105-T139 (TMH3), P150-L173 (TMH4), D192-R223 (TMH5), E340-P369 (TMH6), and L380-K405 (TMH7). The helical part of the rat 5-HT$_{1A}$ receptor was modeled by homology, using bovine rhodopsin as a structural template.

Building a protein model always requires several theoretical assumptions and methodological approximations. Therefore to validate the 5-HT$_{1A}$ receptor model, the fully automated docking of the natural ligand 5-HT was undertaken. If the structure of the putative binding site is correct, then a docking study should be able to detect the proper binding mode for high-affinity ligands, reflecting most of the experimentally known favorable interactions [48,49]. The 5-HT was correctly positioned into the inner part of the seven-helix bundle and the fundamental ligand–protein interactions

suggested by the mutagenesis data were detected. 5-HT formed an ionic interaction with its protonated nitrogen and the negatively charged carboxy terminus of the highly conserved D116 in TMH3. Moreover 5-hydroxy group of 5-HT was placed in a favorable position to form hydrogen bonds with S199 and T200 in TMH5. Finally, an aromatic stacking between the aromatic rings of 5-HT, F361 and F362 was observed.

Since the conformation of α-helices located in hydrophilic environments, such as water, differs from the conformation of α-helices located in hydrophobic environments, such as the cell membrane [50], the transmembrane domain containing 5-HT ligand located in the putative binding site was subjected to the optimization in a strongly hydrophobic environment. The optimization was carried out by immersing the protein into a hydrophobic environment formed by methane molecules and performed rigid body molecular dynamics. Explicit methane molecules were supposed to mimic an environment that is not able to form hydrogen bonds with the peptide carbonyl oxygen of a helix. A significant change in the conformation of the α-helix depending whether the peptide bond is exposed to bulk of water or to the lipid membrane has already been studied by molecular dynamics simulations in the box of methane as well as by surveying crystal structures of membrane proteins [26]. Furthermore, it has been proved that the simulation in the methane environment reproduces the dihedral angles profile of the Pro kink observed in the analysis of crystal structures, indicating that the methane box can reproduce the conformational behavior of helical deformations as well [26]. Similar conditions have been employed to mimic the membrane environment in molecular dynamics simulations of the potassium channel [27], thyrotropin receptor [28] as well as individual TMHs of the CCR5 [29] and 5-HT$_{1A}$ [30] receptors.

Time-dependent changes in RMS displacement of Cα atoms as well as in the total hydrophobic surface area (ASA$_H$) of seven-helix bundle during 500 ps of MD simulation in the presence of explicit methane molecules are shown in Fig. 1. Both parameters reached an equilibrium state after circa 200 ps, fluctuating around a constant mean value. This is sufficient to indicate successful optimization of the translational and rotational orientation of the helices in strongly hydrophobic environment.

The loops and terminal fragments were connected to the transmembrane domain and the entire model was further energy refined by MD simulation. Since no disulfide connectivity existence was detected for the ICL3 sequence, only one disulfide bond between C109 in TMH3 and C187 in ECL2 was present during all simulations. The overall structure of energy-refined 5-HT$_{1A}$ receptor model is shown in Fig. 2. Both extra- and intracellular domain adopted a compact structure with the mainly negative electrostatic potentials observed around the extracellular parts and mainly positive around the intracellular parts. It was suggested that the negatively charged area outside the extracellular parts initiates agonist binding to the 5-HT$_{1A}$ receptor by electrostatic interactions with the protonated basic nitrogen of a ligand [64]. Moreover, the predicted binding site (shown in Fig. 2 as a molecular surface) was found to be in excellent agreement with the residues determined experimentally to be involved in binding.
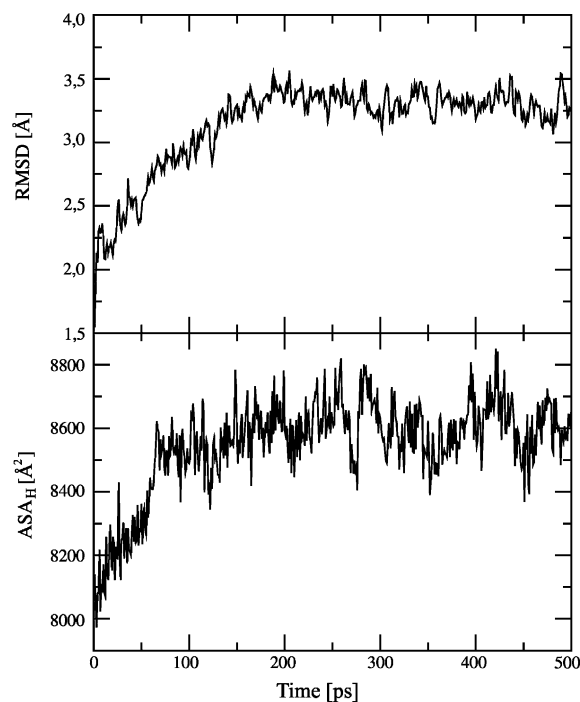

Fig. 1 – The α-carbon RMSD from the starting structure and the total hydrophobic surface area (ASA$_H$) plotted as a function of simulation time for the 5-HT$_{1A}$ transmembrane domain in methane.

The R- and S-8-OH-DPAT were docked into the putative active site of 5-HT$_{1A}$ receptor and 1 ns of unconstrained MD simulations were carried out. Additional MD simulations of both ligand–receptor complexes with the ligands constrained by a very weak potential were performed in order to investigate the trajectories devoid of the substantial variations of ligands geometries.

3.1.2. Conformational analyses of ligands

The initial structures of protonated R- and S-8-OH-DPAT obtained by the geometry optimization differ with respect to the position of the basic nitrogen atom relative to the tetraline ring. Differences in the overall conformations occur in the orientations of the di-n-propylamino moieties as a consequence of the opposite chiralities of the C2 carbon. In R-enantiomer the basic nitrogen atom is positioned equatorial at the tetraline ring, whereas in S the nitrogen atom is oriented in an axial fashion. Moreover, the C1–C2–N–H torsion angle calculated for R- and S-8-OH-DPAT was found to be 172.3° and 40.3°, respectively. These results indicate that only the R-enantiomer satisfies well the criteria proposed for a bioactive conformation [65]. The analysis of trajectories revealed that the geometry of R-8-OH-DPAT was maintained during 1 ns of unconstrained MD simulations of ligand–receptor complex, whereas during unconstrained MD simulation of the S-8-OH-DPAT–5-HT$_{1A}$ complex, an interesting distortion in the ligand conformation was observed. After 620 ps the nitrogen atom moved to the position equatorial at the tetraline ring, through an intermediate form appeared in a short time at 570–620 ps (Fig. 3).
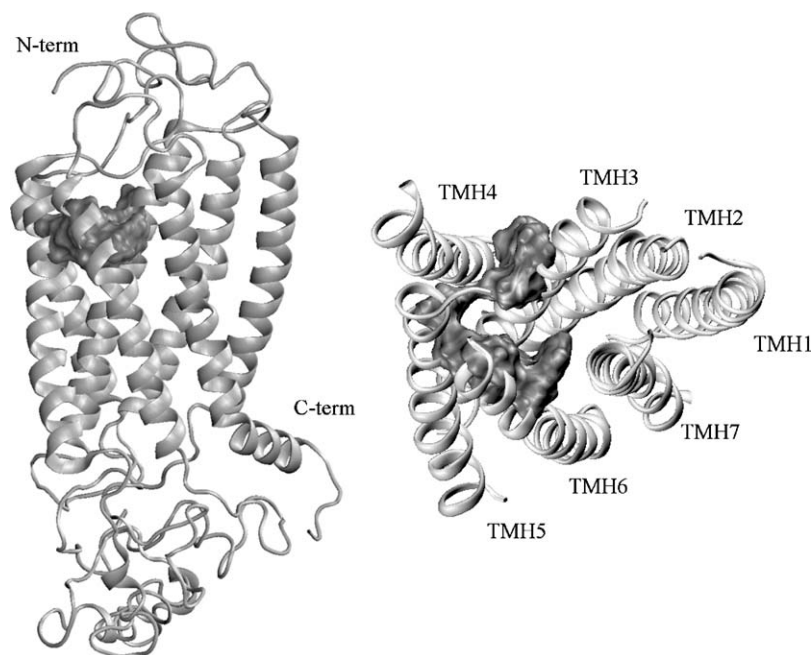
Fig. 2 – Overall structure of the rat 5-HT$_{1A}$ receptor model. Seven TMHs are presented as ribbons, whereas the predicted binding site is shown as a molecular surface (dark grey). Left panel: view along the plane of cell membrane. Right panel: transmembrane domain as viewed from the extracellular side.

The conformation of S-enantiomer bearing equatorial amino substituent requires the energy penalty of 1.88 kcal/mol. Along the last 380 ps of unconstrained MD of both R- and S-8-OH-DPAT–5-HT$_{1A}$ complexes, the hydroxy substituent, the aromatic nuclei and the protonated nitrogen atoms were oriented in a similar fashion and strongly resembled the pharmacophore model. It is noteworthy that the conformation of S-8-OH-DPAT bearing equatorial amino substituent was not observed during docking exploration procedure before MD simulation.
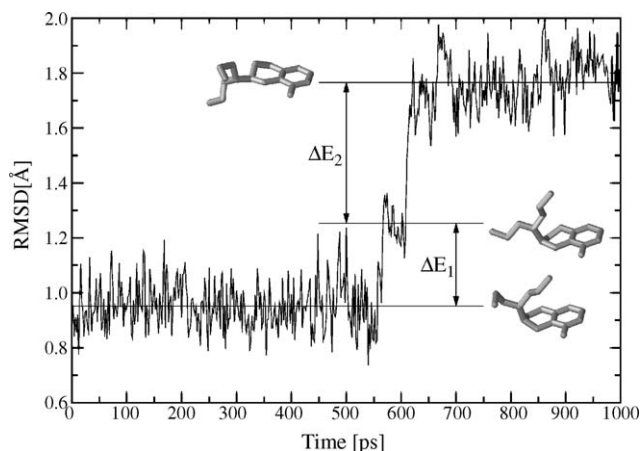

Fig. 3 – The average RMSD from the optimized structure for S-8-OH-DPAT during MD simulation of the ligand–receptor complex. The distortion energies (ΔE_1 = 0.48 kcal/mol and ΔE_2 = 1.04 kcal/mol) were calculated for energy-minimized average structures of the ligand (shown in sticks representation) along 0–570, 570–620 and 620–1000 ps.

3.1.3. Binding pockets for R- and S-8-OH-DPAT

The amino acids remaining in the close vicinity of R- and S-8-OH-DPAT bound to the rat 5-HT$_{1A}$ receptor in the energy-minimized average complexes after MD simulations are shown in Table 1. Moreover, the positions of side chains surrounding both enantiomers are depicted in Fig. 4. The predicted binding sites were found to be in excellent agreement with the residues determined experimentally to be involved in binding [48,49].

All G-protein-coupled monoaminergic receptors contain a highly conserved aspartic acid residue at similar positions in TMH3, corresponding to D116 in the 5-HT$_{1A}$ receptor. Site-directed mutagenesis studies have revealed that mutation of this residue in D$_2$ receptor to an uncharged one completely abolishes the binding of both receptor agonists and antagonists [66], strongly suggesting that the negatively charged carboxy terminus of the aspartic acid is involved in forming a reinforced electrostatic interaction with the protonated, positively charged nitrogen atom of natural and synthetic receptor ligands. Although the overall orientations of R- and S-8-OH-DPAT within the binding site were not identical, both enantiomers formed a reinforced electrostatic interaction with their protonated nitrogens and D116.

Furthermore, the hydroxyl group present in the chemical structure of many neurotransmitters seems to hydrogen bond a series of Ser/Thr residues in TMH5 [67]. A serine (S199) and threonine (T200) residue in TMH5 of the 5-HT$_{1A}$ receptor are both capable of forming hydrogen bonds with the 5-hydroxy group of 5-HT. The 5-hydroxy substituent of 5-HT may act as a hydrogen bond acceptor, since the methoxy analogues of 5-HT and hydroxy-containing synthetic 5-HT$_{1A}$ receptor agonists are usually equipotent. The importance of T200 for 5-HT binding was supported by site-directed

Table 1 – Residues within 5 Å of R- and S-8-OH-DPAT bound to the rat 5-HT$_{1A}$ receptor model

Ligand	Receptor domain	Amino acid residue
R-8-OH-DPAT	TMH3	F112, **I113, D116, V117**, C120, T121
	TMH4	P171
	ECL2	**W175**, T188, **I189, S190**
	TMH5	Y195, **T196**, **S199**, **T200**, A203, F204
	TMH6	**F361, F362, V364, A365**, L368, P369
	ECL3	M377
	TMH7	**I385, N386**, Y390
R-8-OH-DPAT (ligand-constrained)	TMH2	Y96
	TMH3	**F112**, I113, **D116, V117**, C120, T121
	ECL2	**W175, I189, S190**
	TMH5	Y195, **T196, S199, T200**, A203, F204
	TMH6	**F361, F362, V364, A365**, L368, **P369**
	ECL3	M377
	TMH7	G382, **I385, N386**, Y390
S-8-OH-DPAT	TMH2	Y96
	TMH3	F112, **I113, D116, V117, C120, T121**
	TMH4	P171
	ECL2	W175, T188, **I189**
	TMH5	T196, **S199, T200, A203**, F204
	TMH6	**F361, F362**, V364, **A365**, P369
	ECL3	M377
	TMH7	I385, **N386**, Y390
S-8-OH-DPAT (ligand-constrained)	TMH3	**I113, D116, V117**, C120, **T121**
	TMH4	**I167**
	ECL2	**I189**, S190
	TMH5	T196, **S199, T200, A203**
	TMH6	W358, **F361, F362**, V364, **A365**, L368, **P369**
	ECL3	M377
	TMH7	G382, **I385**, N386

The residues within 3 Å are distinguished in bold.

mutagenesis studies [49]. A bifurcated hydrogen bond was observed between the hydroxy substituent of both 8-OH-DPAT enantiomers and side chains of S199 and T200, thus confirming the role of these amino acids during the binding process.

Additionally, the binding sites of both enantiomers of 8-OH-DPAT also included residues of TMH6 and TMH7 that experimental studies on dopamine D$_2$ [68] and β$_2$-adrenergic [69] receptors have demonstrated to be ligand accessible. The

mutation studies have shown that phenylalanine residues in TMH6 are crucial for ligand binding [70]. An *edge-to-face* aromatic stacking between the aromatic ring of both enantiomers of 8-OH-DPAT and F361 and F362 were maintained during the unconstrained MD simulations, presumably contributing to the affinity by hydrophobic interactions. Such interactions between S-8-OH-DPAT and aromatic residues of TMH6 were abolished by imposing the constraints on the ligand during the MD simulation.
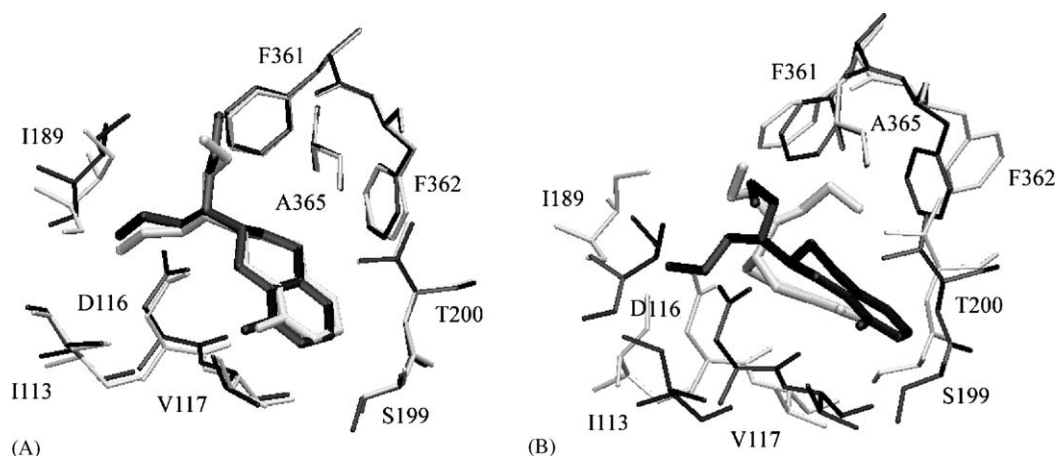

Fig. 4 – Close view on the binding pocket for R-8-OH-DPAT (A) and S-8-OH-DPAT (B) in energy-minimized average structures of the ligand–receptor complexes after unconstrained (black) and ligand-constrained (grey) MD simulations.

Finally, the hydrophobic interactions were detected between the di-n-propyl substituents of both enantiomers and the side chains of residues localized in ECL2 (Table 1). Site-directed mutagenesis experiments and molecular modeling studies have demonstrated that certain residues in ECL2 are important for binding of ligands to the dopamine D_2 [71], α_{1A} adrenergic [72] and adenosine receptors [73]. A direct contact between ligands and residues in ECL2 is possible due to the presence of a disulfide bridge formed between C109 in TMH3 and C187 in ECL2 [60,61], which would covalently attach the ECL2 in physical proximity to the ligand binding site [73]. In addition, the ECL2 was proposed to enter into the binding site crevice of biogenic amine receptors and form a lid over the bound ligand [25]. Interestingly, the single residue of ECL3 constantly remaining in the vicinity of a ligand was observed in all MD trajectories of ligand–receptor complexes (Table 1). An indirect role of ECLs in the formation of a channel for ligand entrance to the primary binding site within helical bundle was suggested [74].

During the unconstrained as well as ligand-constrained MD trajectories, both enantiomers of 8-OH-DPAT remained constantly trapped in a cavity localized in the inner part of the seven-helix bundle of 5-HT_{1A} receptor. However, as can be seen in Fig. 4, even in corresponding sites with each enantiomer anchored by the same receptor residues, they did not have identical binding modes. In addition, the constraints imposed on the S-enantiomer significantly affected the overall conformation of the binding site.

3.1.4. Estimated free energy of binding and affinity value of R- and S-8-OH-DPAT toward 5-HT_{1A} receptor

The estimated values of free energy of binding (E_{bind}) as well as the values of affinity (K_i) of both enantiomers toward the rat 5-HT_{1A} receptor are presented in Fig. 5. For each enantiomer the conformation resulting from both unconstrained as well as ligand-constrained MD simulation was taken into account during the redocking of the ligand into the central cavity of the receptor model. The results seem to be in qualitative agreement with experiments. Thus, it was reported that in vitro binding affinities of R- and S-enantiomer toward 5-HT_{1A} receptor are 4.1 and 6.1 nM, respectively [11] as well as toward the cloned 5-HT_{1A} receptor (0.47, 0.64 and 0.58 nM, for R-, S- and R,S-8-OH-DPAT, respectively) [12]. Moreover, the introduction of constraints on a ligand during MD simulations of ligand–receptor complexes produced significant changes in the affinity of S-enantiomer toward the receptor. A constrained S-8-OH-DPAT further displayed significantly lower affinity for the 5-HT_{1A} receptor (41.37 ± 5.23 nM) than unconstrained (12.71 ± 1.54 nM), whereas the affinities analogically estimated for R-enantiomer were found to be comparable (2.17 ± 0.31 and 1.39 ± 0.14 nM, respectively). Additionally, the values of the free energy of binding to the 5-HT_{1A} receptor were found to be similar for both enantiomers (Fig. 5). The conformational analysis of the distortion of S-8-OH-DPAT geometry during unconstrained MD simulation (Fig. 3) revealed that the orientation bearing equatorial amino substituent can be adopted. This may explain the similarities of the free energy of binding and affinity of R- and S-8-OH-DPAT toward the 5-HT_{1A} receptor reported by experiments [11,12].
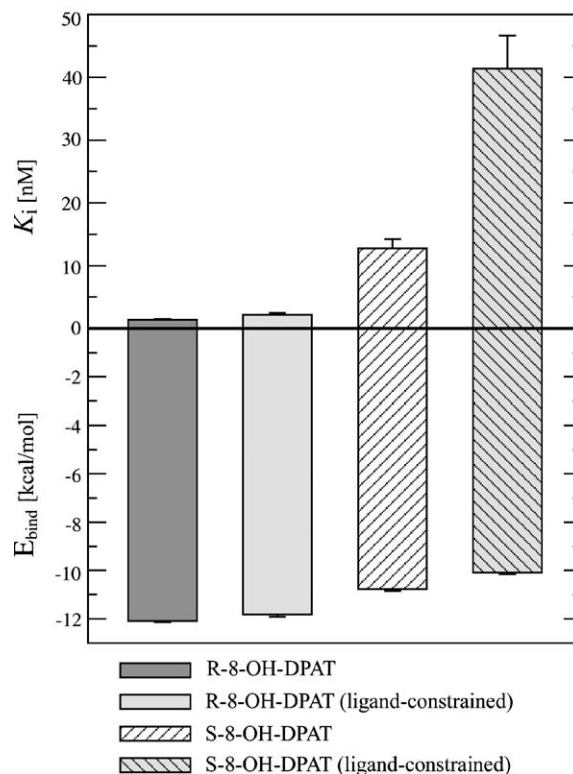

Fig. 5 – Estimated affinities (K_i) toward the 5-HT_{1A} receptor and the values of the free energy of binding (E_{bind}) for R- and S-8-OH-DPAT.

3.1.5. Structural differences between ligand–receptor complexes

A significant difference between the energy-minimized average structures of receptor–ligand complexes after MD simulations was observed. The RMS displacement of receptors' Cα atoms calculated for the R-8-OH-DPAT–5-HT_{1A} versus S-8-OH-DPAT–5-HT_{1A} after unconstrained MD was found to be 3.533 Å (Fig. 6). The corresponding value of RMSD-Cα calculated exclusively for part of the intracellular domain including ICL2, ICL3 and C-terminal tail is 4.721 Å. Since this domain is known to be responsible for G-protein coupling [75], such structural differences may contribute to the efficacy differences for both 8-OH-DPAT enantiomers, reported in biochemical [9,31] as well as behavioral experiments [4,10,15,16].

Although the efficacy of a ligand toward the receptor cannot be estimated quantitatively using the presented model, the structural differences found in the intracellular domain after MD simulations of the 5-HT_{1A} receptor complexed with R- and S-8-OH-DPAT suggest substantial differences in G-protein coupling. Therefore it may be concluded that the intrinsic activities of R- and S-enantiomer toward 5-HT_{1A} receptor are different. It is also noteworthy that the differences in the intracellular domain conformation were observed after both unconstrained as well as ligand-constrained MD simulations. In addition, the constraints imposed on both enantiomers significantly affected the overall conformation of the receptor as well as the TMHs domain.
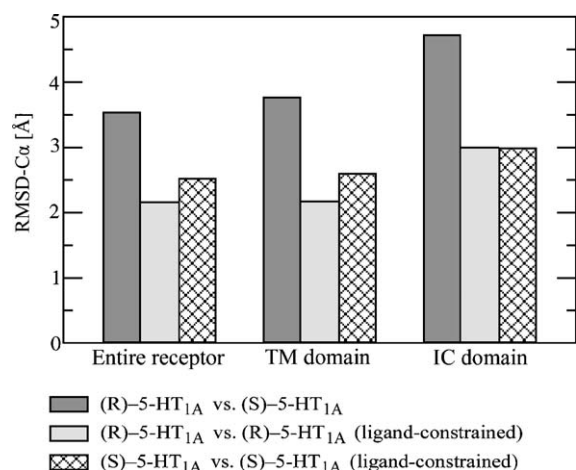
Fig. 6 – RMS differences of the entire receptor and individual domains (TM: transmembrane domain, IC: part of the intracellular domain including ICL2, ICL3 and C-terminal) calculated for energy-minimized average structures of the receptor complexed with R- and S-8-OH-DPAT [denoted as (R)-5-HT$_{1A}$ and (S)-5-HT$_{1A}$, respectively].

3.2. Biochemical experiment

3.2.1. 5-HT synthesis rate in discrete parts of the brain

Activation of 5-HT$_{1A}$ receptors by specific agonists, e.g. prototypical 8-OH-DPAT [1], reveals inhibitory action on serotonergic cell firing and consequently decreases synthesis of 5-HT in raphe nuclei and serotonergic projection areas [20,21]. In chromatographic assay of 5-HT synthesis rate relatively low doses of 8-OH-DPAT pharmacophores were used. However, they were chosen to act exclusively via 5-HT$_{1A}$ autoreceptors and to reveal any possible subtle difference between these compounds' biochemical profiles on the level at presynaptic receptors. R-8-OH-DPAT (0.05, 0.1 mg/kg) as well as R,S-8-OH-DPAT (0.05, 0.1 mg/kg) caused a significant, similar reduction of 5-HT synthesis rate in CA ($p < 0.02$ in comparison to saline-treated rats, Fig. 7A), PFC ($p < 0.02$, Fig. 7B) and BS ($p < 0.05$, Fig. 7C), hence 0.05 mg/kg was a sufficient dose for both compounds to attenuate 5-HT synthesis rate and higher dose did not intensify inhibitory effect on 5-HT synthesis in above brain's structures. S-8-OH-DPAT (0.05, 0.1 mg/kg) was unable to significantly attenuate 5-HT synthesis rate in the mentioned structures, although in brainstem statistical significance was almost reached for S-8-OH-DPAT 0.1 mg/kg ($p = 0.06$). Results derived from CA, PFC and BS confirmed that R-8-OH-DPAT acts as full and potent agonist, whereas S-form, even as a partial agonist, is unable to affect 5-HT synthesis rate in both doses tested. Simultaneously racemic 8-OH-DPAT is equally potent as R-form in 5-HT synthesis rate inhibition in above brain regions.

Administration of R-8-OH-DPAT 0.05 mg/kg caused also significant reduction of 5-HT synthesis rate in the HP ($p < 0.02$ in comparison to saline-treated animals, Fig. 7D), whereas racemic 8-OH-DPAT in both doses failed to decrease 5-HT synthesis rate in that brain region. Interestingly, the difference between R-8-OH-DPAT 0.05 mg/kg and racemic 8-OH-DPAT appeared in brain region which is known to be innervated
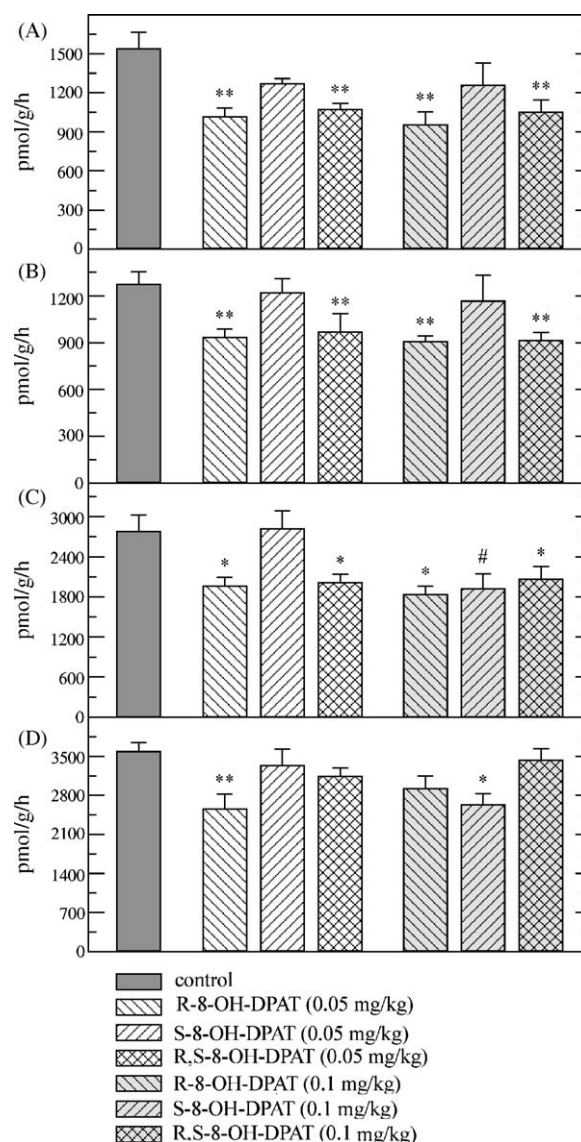

Fig. 7 – 5-HT synthesis rates (pmol/g/h, expressed as means ± S.E.M., $n = 6$–12) after saline, R-8-OH-DPAT (0.05, 0.1 mg/kg), S-8-OH-DPAT (0.05, 0.1 mg/kg) or R,S-8-OH-DPAT (0.05, 0.1 mg/kg) injection in hippocampus (A), prefrontal cortex (B), brainstem (C) and hypothalamus (D) of rat's brain. 5-HT synthesis rates were estimated by chromatographic assay of L-5-HTP level after NSD 1015 (100 mg/kg) administration; $^{*}p < 0.05$, $^{**}p < 0.02$, $^{\#}p = 0.06$ compared to saline-treated rats by analysis of variance (ANOVA one-way) followed by Newman–Keul's for post hoc analysis.

mainly by serotonergic projections from MRN, in opposite to PFC innervated mainly by ascending projections from DRN, BS, which contains both midbrain raphe nuclei and CA innervated by DRN and MRN [76]. Such a finding suggests that R,S-8-OH-DPAT at those doses is insufficient to decrease 5-HT synthesis rates in HP, since it was established that 5-HT$_{1A}$ receptors located on MRN 5-HT neurons are less sensitive to specific agonist than DRN 5-HT$_{1A}$ receptors [77,78]. Therefore it cannot be excluded that lower doses of both stereoisomers could

reveal such difference also in brain regions innervated by DRN. It could not also be ruled out that higher doses of both enantiomers would have had more robust effects, however there were no trends in this direction. However, S-8-OH-DPAT 0.1 mg/kg was able to significantly inhibit 5-HT synthesis rate in HP ($p < 0.05$), whereas R-8-OH-DPAT 0.1 mg/kg failed to evoke such effect in this area (Fig. 7D). Therefore S-8-OH-DPAT 0.1 mg/kg induced attenuation of 5-HT synthesis rate in HP argues against assumption that R,S-8-OH-DPAT does not contain sufficient amount of the active R-isomer capable to evoke such effect in HP. Since 5-HT synthesis rate attenuation is related to 5-HT$_{1A}$ receptor activation, non-specific action of S-8-OH-DPAT can also be excluded. However, the intrinsic activity and potency of 5-HT$_{1A}$ receptor agonist are dependent on receptor density and may vary for different second messenger systems. It is known that 5-HT$_{1A}$ receptor can interact with several different signal transduction pathways and several G-proteins present in different concentrations in various brain regions and thus may cause varying ability to couple the receptor to a particular effector protein. This may explain the large variation in the same agonist potency [79]. The molecular modeling part of this study also revealed structural differences in the intracellular domain responsible for G-protein coupling after MD simulations of the 5-HT$_{1A}$ receptor complexed with R- and S-8-OH-DPAT. It may suggest substantial differences in G-protein coupling, which may finally lead to differences in the intrinsic activities of R- and S-enantiomer toward 5-HT$_{1A}$ receptor in various brain structures, depending on the effector system, 5-HT$_{1A}$ receptors density as well as different transduction system [80]. Thus it may be concluded that in HP S-8-OH-DPAT can act even as full agonist. On the other hand S-8-OH-DPAT was completely unable to affect 5-HT synthesis rate in brain regions innervated by DRN serotonergic neurons PFC and CA innervated by both DRN and MRN. It argues against hypothesis that even a weak partial agonist could suppress serotonergic transmission via these receptors due to higher 5-HT$_{1A}$ receptors' reserve in DRN [81].

Previous biochemical findings are mostly compatible with the results presented in this paper, since in electrophysiological measurements S-isomer had about three-fold lower potency than R-isomer to inhibit electrical activity of DRN serotonergic neurons, whereas R,S-8-OH-DPAT showed intermediate activity [12]. In the microdialysis study conducted by Yoshitake and Kehr [4] R-enantiomer (0.3 mg/kg) was about twice more potent in reducing the extracellular 5-HT level in ventral hippocampus than its S-counterpart (0.3 mg/kg); however, R-8-OH-DPAT administered at the same dose as racemate reduced 5-HT level only by additional 6–10% more than the latter. Similar findings were found in hypothermic study by the above authors, since significant differences between the hypothermic effects of racemate or R-8-OH-DPAT compared to S-isomer at both doses tested (0.1, 0.3 mg/kg) were reported. The racemate and its R-counterpart showed almost identical profile of hypothermic effect. S-Isomer was about 50% less potent than R and R,S to induce hypothermia. Yoshitake and Kehr [4] therefore concluded that R and R,S are almost equally potent in reduction of body temperature and 5-HT release in ventral hippocampus, which is consistent with our experiment since R- and R,S-8-OH-DPAT had equal potencies in inhibiting 5-HT synthesis rate in CA, PFC and

BS. Such lack of the difference between R-isomer and racemate results probably from the relatively high doses of R,S-8-OH-DPAT used, because it presumably contains sufficient amount of active, R-form capable to evoke the biochemical as well as hypothermic effect.

4.   Conclusions

The results of the present study emphasized the stereoselectivity of 8-OH-DPAT toward the serotonin 5-HT$_{1A}$ receptor. The molecular modeling strategy allowed a reliable 3D model of the rat 5-HT$_{1A}$ receptor to be constructed from the amino acid sequence using the crystal structure of bovine rhodopsin as a structural template. The structure of the receptor model was validated through docking studies and molecular dynamics simulations that gave results consistent with experimental data. Docking studies and the dynamics of ligand–receptor complexes revealed the distortion of S-8-OH-DPAT geometry during unconstrained MD simulation. The conformation of S-enantiomer bearing equatorial amino substituent may explain the similarities of the free energy of binding and affinity of R- and S-8-OH-DPAT toward the 5-HT$_{1A}$ receptor reported by autoradiographic experiments. However, a significant difference between the energy-minimized average structures of receptor–ligand complexes (especially within the part of the domain responsible for G-protein coupling) after MD simulations may contribute to the efficacy differences for both 8-OH-DPAT enantiomers. Based on the presented results it might be possibly explained that R-8-OH-DPAT acts as a full, potent agonist, whereas S-8-OH-DPAT requires a structural distortion to the active potent form of this compound. Racemic 8-OH-DPAT could in fact behave as a potent or less potent agonist according to the dose used and the brain region being investigated due to the greater sensitivity of 5-HT$_{1A}$ receptors located in DRN to 8-OH-DPAT. Therefore according to previous findings and the results presented in this paper the biochemical as well as behavioral effects evoked by the racemic form can be similar or slightly less significant than elicited by pure R-enantiomer. On the other hand it should be emphasized that at the level at presynaptic 5-HT$_{1A}$ receptors, such difference could occur, especially in brain areas innervated by MRN. The similar effects of R-enantiomer and racemate observed in PFC, CA and BS in the biochemical experiment might result from still high dose of R,S-8-OH-DPAT used and/or the capability of racemate to act as a full potent R-isomer, since its S-counterpart is able to distort to the structural-active pharmacophore. However, even assuming the equal potencies of R- and R,S-8-OH-DPAT in brain structures innervated by DRN, it may be better to avoid using the racemic form in areas less sensitive to 5-HT$_{1A}$ agonist.

Although S-8-OH-DPAT was reported to have partial agonistic property at 5-HT$_{1A}$ receptors, it was unable at both doses tested to significantly inhibit 5-HT synthesis rate in all examined brain areas, with exception of HP. The results may indicate the different sensitivity of particular brain's regions to 5-HT$_{1A}$ agonist, especially in area innervated by MRN serotonergic projections, since S-8-OH-DPAT was able to evoke inhibitory effect on 5-HT synthesis in HP. The results of both biochemical and computational studies confirmed that R-enantiomer in contrast to S-8-OH-DPAT acts as a full and

potent agonist, whilst the racemic form may display similar pharmacological profile to R-8-OH-DPAT.

Acknowledgements

REFERENCES

[1] Arvidsson LE, Hacksell U, Nilsson JL, Hjorth S, Carlsson A, Lindberg P, et al. 8-Hydroxy-2-(di-n-propylamino)tetralin, a new centrally acting 5-hydroxytryptamine receptor agonist. J Med Chem 1981;24(8):921–3.

[2] Brambilla A, Baschirotto A, Grippa N, Borsini F. Effect of flibanserin (BIMT 17), fluoxetine, 8-OH-DPAT and buspirone on serotonin synthesis in rat brain. Eur Neuropsychopharmacol 1999;10(1):63–7.

[3] Amargos-Bosch M, Adell A, Bortolozzi A, Artigas F. Stimulation of alpha1-adrenoceptors in the rat medial prefrontal cortex increases the local in vivo 5-hydroxytryptamine release: reversal by antipsychotic drugs. J Neurochem 2003;87(4):831–42.

[4] Yoshitake T, Kehr J. Differential effects of (R)-, (R,S)- and (S)-8-hydroxy-2-(di-n-propylamino)tetralin on hippocampal serotonin release and induction of hypothermia in awake rats. Life Sci 2004;74(23):2865–75.

[5] Ebenezer IS. Effects of the 5HT1A agonist, 8-OH-DPAT, on operant food intake in non-deprived rats. Neuroreport 1992;3(1):62–4.

[6] Testa R, Guarneri L, Poggesi E, Angelico P, Velasco C, Ibba M, et al. Effect of several 5-hydroxytryptamine (1A) receptor ligands on the micturition reflex in rats: comparison with WAY 100635. J Pharmacol Exp Ther 1999;290(3):1258–69.

[7] Prow MR, Martin KF, Heal DJ. 8-OH-DPAT-induced mydriasis in mice: a pharmacological characterisation. Eur J Pharmacol 1996;317(1):21–8.

[8] Millan MJ, Bervoets K, Colpaert FC. 5-Hydroxytryptamine (5-HT)1A receptors and the tail-flick response. I. 8-Hydroxy-2-(di-n-propylamino)tetralin HBr-induced spontaneous tail-flicks in the rat as an in vivo model of 5-HT1A receptor-mediated activity. J Pharmacol Exp Ther 1991;256(3):973–82.

[9] Cornfield LJ, Lambert G, Arvidsson LE, Mellin C, Vallgarda J, Hacksell U, et al. Intrinsic activity of enantiomers of 8-hydroxy-2-(di-n-propylamino)tetralin and its analogs at 5-hydroxytryptamine1A receptors that are negatively coupled to adenylate cyclase. Mol Pharmacol 1991;39(6):780–7.

[10] Hadrava V, Blier P, de Montigny C. Partial agonistic activity of R- and S-enantiomers of 8-OH-DPAT at 5-HT1A receptors. J Psychiatry Neurosci 1996;21(2):101–8.

[11] Hacksell U, Liu Y, Yu H, Vallgarda J, Hook BB, Johansson AM, et al. Neuromedicinal chemistry of 5-HT1A-receptor agonists and antagonists. Drug Des Discov 1993;9(3–4):287–97.

[12] Lejeune F, Newman-Tancredi A, Audinot V, Millan MJ. Interactions of (+)- and (−)-8- and 7-hydroxy-2-(di-n-propylamino)tetralin at human (h)D3, hD2 and h serotonin1A receptors and their modulation of the activity of serotoninergic and dopaminergic neurones in rats. J Pharmacol Exp Ther 1997;280(3):1241–9.

[13] Arvidsson LE, Hacksell U, Johansson AM, Nilsson JL, Lindberg P, Sanchez D, et al. 8-Hydroxy-2-(alkylamino)tetralins and related compounds as central 5-hydroxytryptamine receptor agonists. J Med Chem 1984;27(1):45–51.

[14] Bjork L, Hook BB, Nelson DL, Anden NE, Hacksell U. Resolved N,N-dialkylated 2-amino-8-hydroxytetralins: stereoselective interactions with 5-HT1A receptors in the brain. J Med Chem 1989;32(4):779–83.

[15] Cao BJ, Rodgers RJ. Different behavioural profiles of the R(+)- and S(−)-enantiomers of 8-hydroxy-2-(di-n-propylamino)tetralin in the murine elevated plus-maze. Behav Pharmacol 1996;7(8):810–9.

[16] Honda M, Ono H. Differential effects of (R)- and (S)-8-hydroxy-2-(di-n-propylamino)tetralin on the monosynaptic spinal reflex in rats. Eur J Pharmacol 1999;373(2–3):171–9.

[17] Zuideveld KP, Treijtel N, Van der Graaf PH, Danhof M. Enantioselective high-performance liquid chromatographic analysis of the 5-HT1A receptor agonist 8-hydroxy-2-(di-n-propylamino)tetralin. Application to a pharmacokinetic–pharmacodynamic study in rats. J Chromatogr B Biomed Sci Appl 2000;738(1):67–73.

[18] Barnes NM, Sharp T. A review of central 5-HT receptors and their function. Neuropharmacology 1999;38(8):1083–152.

[19] Hamon M. The main features of central 5-HT1A receptors. In: Baumgarten HG, Gothert M, editors. Serotonergic neurons and 5-HT receptors in the CNS. Berlin: Springer-Verlag; 2000. p. 239–68.

[20] Pineyro G, Blier P. Autoregulation of serotonin neurons: role in antidepressant drug action. Pharmacol Rev 1999;51(3):533–91.

[21] Blier P, Pineyro G, el Mansari M, Bergeron R, de Montigny C. Role of somatodendritic 5-HT autoreceptors in modulating 5-HT neurotransmission. Ann NY Acad Sci 1998;861:204–16.

[22] Carlsson A, Davis JN, Kehr W, Lindquist M, Aback CV. Simultaneous measurement of tyrosine and tryptophan hydroxylase activities in brain in vivo using an inhibitor of the aromatic amino acid decarboxylase. Naunyn Schmiedebergs Arch Pharmacol 1972;275:153–68.

[23] Palczewski K, Kumasaka T, Hori T, Behnke CA, Motoshima H, Fox BA, et al. Crystal structure of rhodopsin: a G protein-coupled receptor. Science 2000;289(5480):739–45.

[24] Visiers I, Ballesteros JA, Weinstein H. Three-dimensional representations of G protein-coupled receptor structures and mechanisms. Meth Enzymol 2002;343:329–71.

[25] Kristiansen K. Molecular mechanisms of ligand binding, signaling, and regulation within the superfamily of G-protein-coupled receptors: molecular modeling and mutagenesis approaches to receptor structure and function. Pharmacol Ther 2004;103(1):21–80.

[26] Olivella M, Deupi X, Govaerts C, Pardo L. Influence of the environment in the conformation of α-helices studied by protein database search and molecular dynamics simulations. Biophys J 2002;82:3207–13.

[27] Aqvist J, Luzhkov V. Ion permeation mechanism of the potassium channel. Nature 2000;404(6780):881–4.

[28] Govaerts C, Lefort A, Costagliola S, Wodak SJ, Ballesteros JA, Van Sande J, et al. A conserved Asn in transmembrane helix 7 is an on/off switch in the activation of the thyrotropin receptor. J Biol Chem 2001;276(25):22991–9.

[29] Govaerts C, Blanpain C, Deupi X, Ballet S, Ballesteros JA, Wodak SJ, et al. The TXP motif in the second transmembrane helix of CCR5. A structural determinant of

chemokine-induced activation. J Biol Chem 2001;276(16):13217–25.

[30] Lopez-Rodriguez ML, Vicente B, Deupi X, Barrondo S, Olivella M, Morcillo MJ, et al. Design, synthesis and pharmacological evaluation of 5-hydroxytryptamine (1a) receptor ligands to explore the three-dimensional structure of the receptor. Mol Pharmacol 2002;62(1):15–21.

[31] Pauwels PJ, Colpaert FC. Stereoselectivity of 8-OH-DPAT enantiomers at cloned human 5-HT1D receptor sites. Eur J Pharmacol 1996;300(1–2):137–9.

[32] Yu H, Liu Y, Malmberg A, Mohell N, Hacksell U, Lewander T. Differential serotoninergic and dopaminergic activities of the (R)- and the (S)-enantiomers of 2-(di-n-propylamino)tetralin. Eur J Pharmacol 1996;303(3):151–62.

[33] Magnusson O, Nilsson LB, Westerlund D. Simultaneous determination of dopamine, DOPAC and homovanillic acid. Direct injection of supernatants from brain tissue homogenates in a liquid chromatography–electrochemical detection system. J Chromatogr 1980;221:237–47.

[34] Pearlman DA, Case DA, Caldwell JW, Ross WR, Cheatham TE, DeBolt IS, et al. AMBER, a computer program for applying molecular mechanics, normal mode analysis, molecular dynamics and free energy calculations to elucidate the structures and energies of molecules. Comp Phys Commun 1995;91:1–41.

[35] Wang J, Cieplak P, Kollman PA. How well does a restrained electrostatic potential (RESP) model perform in calculating conformational energies of organic and biological molecules? J Comput Chem 2000;21(12):1049–74.

[36] Ryckaert JP, Ciccotti G, Berendsen HJC. Numerical integration of the Cartesian equation of motion of a system constraints: molecular dynamics of N-alkanes. J Comput Phys 1977;23:327–41.

[37] Humphrey W, Dalke A, Schulten K. VMD: visual molecular dynamics. J Mol Graph 1996;14(1). 33-8, 27-8.

[38] Goodsell DS, Olson AJ. Automated docking of substrates to proteins by simulated annealing. Proteins 1990;8(3):195–202.

[39] InsightII. San Diego, CA, USA: Molecular Simulations Inc.

[40] Steward JJP. MOPAC Tokyo, Japan: Fujitsu Limited; 1993.

[41] Jakalian A, Bush BL, Jack DB, Bayly CI, Fast. Efficient generation of high-quality atomic charges. AM1-BCC Model. I. Method. J Comput Chem 2000;21:132–46.

[42] Wang J, Wang W, Kollman PA. Antechamber: an accessory software package for molecular mechanical calculations. Abstr Pap J Am Chem Soc 2001;220:135–40.

[43] Wang J, Wolf RM, Caldwell JW, Kollman PA, Case DA. Development and testing of a general amber force field. J Comput Chem 2004;25(9):1157–74.

[44] Albert PR, Zhou QY, Van Tol HH, Bunzow JR, Civelli O. Cloning, functional expression, and mRNA tissue distribution of the rat 5-hydroxytryptamine1A receptor gene. J Biol Chem 1990;265(10):5825–32.

[45] Bairoch A, Apweiler R. The SWISS-PROT protein sequence database and its supplement TrEMBL in 2000. Nucl Acids Res 2000;28:45–8.

[46] Horn F, Bettler E, Oliveira L, Campagne F, Cohen FE, Vriend G. GPCRDB information system for G protein-coupled receptors. Nucl Acids Res 2003;31(1):294–7.

[47] Canutescu AA, Shelenkov AA, Dunbrack Jr RL. A graph-theory algorithm for rapid protein side-chain prediction. Protein Sci 2003;12(9):2001–14.

[48] Chanda PK, Minchin MC, Davis AR, Greenberg L, Reilly Y, McGregor WH, et al. Identification of residues important for ligand binding to the human 5-hydroxytryptamine1A serotonin receptor. Mol Pharmacol 1993;43(4):516–20.

[49] Ho BY, Karschin A, Branchek T, Davidson N, Lester HA. The role of conserved aspartate and serine residues in ligand binding and in function of the 5-HT1A receptor: a site-directed mutation study. FEBS Lett 1992;312(2–3):259–62.

[50] White SH, Wimley WC. Membrane protein folding and stability: physical principles. Annu Rev Biophys Biomol Struct 1999;28:319–65.

[51] Darden T, York D, Pedersen L. Particle mesh Ewald. An N log(N) method for Ewald sumsin large systems. J Chem Phys 1993;98:10089–92.

[52] Jeffrey GA. An introduction to hydrogen bonding New York: Oxford University Press; 1997.

[53] Eisenberg D, Schwarz E, Komaromy M, Wall R. Analysis of membrane and surface protein sequences with the hydrophobic moment plot. J Mol Biol 1984;179(1):125–42.

[54] Xiang Z, Honig B. Extending the accuracy limits of prediction for side-chain conformations. J Mol Biol 2001;311(2):421–30.

[55] Sali A, Blundell TL. Comparative protein modelling by satisfaction of spatial restraints. J Mol Biol 1993;234(3):779–815.

[56] Higgins DG, Sharp PM. CLUSTAL: a package for performing multiple sequence alignment on a microcomputer. Gene 1988;73(1):237–44.

[57] DePristo MA, de Bakker PI, Lovell SC, Blundell TL. Ab initio construction of polypeptide fragments: efficient generation of accurate, representative ensembles. Proteins 2003;51(1):41–55.

[58] Kim DE, Chivian D, Baker D. Protein structure prediction and analysis using the Robetta server. Nucl Acids Res 2004;32(Web Server issue):W526–31.

[59] Fariselli P, Casadio R. Prediction of disulfide connectivity in proteins. Bioinformatics 2001;17(10):957–64.

[60] Dohlman HG, Caron MG, DeBlasi A, Frielle T, Lefkowitz RJ. Role of extracellular disulfide-bonded cysteines in the ligand binding function of the beta 2-adrenergic receptor. Biochemistry 1990;29(9):2335–42.

[61] Noda K, Saad Y, Graham RM, Karnik SS. The high affinity state of the beta 2-adrenergic receptor requires unique interaction between conserved and non-conserved extracellular loop cysteines. J Biol Chem 1994;269(9):6743–52.

[62] Farrens DL, Altenbach C, Yang K, Hubbell WL, Khorana HG. Requirement of rigid-body motion of transmembrane helices for light activation of rhodopsin. Science 1996;274(5288):768–70.

[63] Strzelczyk AA, Jaronczyk M, Chilmonczyk Z, Mazurek AP, Chojnacka-Wojcik E, Sylte I. Intrinsic activity and comparative molecular dynamics of buspirone analogues at the 5-HT (1A) receptors. Biochem Pharmacol 2004;67(12):2219–30.

[64] Sylte I, Bronowska A, Dahl SG. Ligand induced conformational states of the 5-HT (1A) receptor. Eur J Pharmacol 2001;416(1–2):33–41.

[65] Hibert MF, McDermott I, Middlemiss DN, Mir AK, Fozard JR. Radioligand binding study of a series of 5-HT1A receptor agonists and definition of a steric model of this site. Eur J Med Chem 1989;24:31–7.

[66] Mansour A, Meng F, Meador-Woodruff JH, Taylor LP, Civelli O, Akil H. Site-directed mutagenesis of the human dopamine D2 receptor. Eur J Pharmacol 1992;227(2):205–14.

[67] Strader CD, Candelore MR, Hill WS, Sigal IS, Dixon RA. Identification of two serine residues involved in agonist activation of the beta-adrenergic receptor. J Biol Chem 1989;264(23):13572–8.

[68] Javitch JA, Ballesteros JA, Weinstein H, Chen J. A cluster of aromatic residues in the sixth membrane-spanning segment of the dopamine D2 receptor is accessible in the binding-site crevice. Biochemistry 1998;37(4):998–1006.

[69] Javitch JA, Fu D, Liapakis G, Chen J. Constitutive activation of the beta2 adrenergic receptor alters the orientation of its

sixth membrane-spanning segment. J Biol Chem 1997;272(30):18546–9.

[70] Cho W, Taylor LP, Mansour A, Akil H. Hydrophobic residues of the D2 dopamine receptor are important for binding and signal transduction. J Neurochem 1995;65(5):2105–15.

[71] Shi L, Javitch JA. The second extracellular loop of the dopamine D2 receptor lines the binding-site crevice. Proc Natl Acad Sci USA 2004;101(2):440–5.

[72] Zhao MM, Hwa J, Perez DM. Identification of critical extracellular loop residues involved in alpha 1-adrenergic receptor subtype-selective antagonist binding. Mol Pharmacol 1996;50(5):1118–26.

[73] Kim J, Jiang Q, Glashofer M, Yehle S, Wess J, Jacobson KA. Glutamate residues in the second extracellular loop of the human A2a adenosine receptor are required for ligand recognition. Mol Pharmacol 1996;49(4):683–91.

[74] Schadel SA, Heck M, Maretzki D, Filipek S, Teller DC, Palczewski K, et al. Ligand channeling within a G-protein-coupled receptor. The entry and exit of retinals in native opsin. J Biol Chem 2003;278(27):24896–903.

[75] Cai K, Itoh Y, Khorana HG. Mapping of contact sites in complex formation between transducin and light-activated rhodopsin by covalent crosslinking: use of a photoactivatable reagent. Proc Natl Acad Sci USA 2001;98(9):4877–82.

[76] McQuade R, Sharp T. Functional mapping of dorsal and median raphe 5-hydroxytryptamine pathways in forebrain of the rat using microdialysis. J Neurochem 1997;69(2): 791–6.

[77] Casanovas JM, Artigas F. Differential effects of ipsapirone on 5-hydroxytryptamine release in the dorsal and median raphe neuronal pathways. J Neurochem 1996;67(5):1945–52.

[78] Hajos M, Gartside SE, Villa AE, Sharp T. Evidence for a repetitive (burst) firing pattern in a sub-population of 5-hydroxytryptamine neurons in the dorsal and median raphe nuclei of the rat. Neuroscience 1995;69(1):189–97.

[79] Boess FG, Martin IL. Molecular biology of 5-HT receptors. Neuropharmacology 1994;33(3–4):275–317.

[80] Hoyer D, Boddeke HW. Partial agonists, full agonists, antagonists: dilemmas of definition. Trends Pharmacol Sci 1993;14(7):270–5.

[81] Gobert A, Lejeune F, Rivet JM, Audinot V, Newman-Tancredi A, Millan MJ. Modulation of the activity of central serotoninergic neurons by novel serotonin1A receptor agonists and antagonists: a comparison to adrenergic and dopaminergic neurons in rats. J Pharmacol Exp Ther 1995;273(3):1032–46.